JOURNAL OF AIRCRAFT
Vol. 46, No. 6, November–December 2009

Computational Investigation of Gurney Flap Effects on Rotors in Forward Flight

Byung-Young Min,* Lakshmi N. Sankar,† Nischint Rajmohan,* and J. V. R. Prasad‡
Georgia Institute of Technology, Atlanta, Georgia 30332-0150

DOI: 10.2514/1.41918

A hybrid Navier–Stokes/free-wake solver has been employed to investigate the performance of a rotor equipped with a Gurney flap in steady level flight and in descent. A scaled model of the BO-105 rotor was studied. The calculations were coupled to a comprehensive analysis to properly account for the effects of the elastic deformations on the aerodynamic loads and to account for trim. Fixed and dynamically deployed Gurney flaps were considered. In forward flight, it was found that a properly chosen azimuthal deployment schedule of the Gurney flaps may reduce the peak-to-peak variations in hub loads, potentially reducing vibrations. In descent flight, it was found that the deployment of a fixed Gurney flap decreased the descent rate needed to maintain autorotation.

Nomenclature

C_l = airfoil lift coefficient
C_m = airfoil pitching moment coefficient
C_n = airfoil normal force coefficient
C_P = rotor power coefficient
C_T = rotor thrust coefficient
D = drag
D_e = equivalent drag
GF = Gurney flap
F = force
L = lift
l_G = deployed Gurney flap length
M = Mach number, moment
PL = power loading C_T/C_P
R = blade radius
r = blade radial location
V_∞ = freestream velocity
α = angle of attack
α_s = shaft angle of attack
σ = solidity
Ψ = azimuth angle
Ω = rotor rotational speed

I. Introduction

A GURNEY flap is a passive high-lift device that has applications in many areas ranging from racing cars to helicopters. In its simplest form, it is a small vertical tab attached to the trailing edge of a wing. Because of its high-lift potential, it is being considered for use in vertical-lift systems such as micro unmanned aerial vehicles.

Researchers at the U.S. Army Aeroflightdynamics Directorate have recently conducted a series of tests to understand the physical mechanisms behind the high-lift generation. Static airfoil data as well as dynamic stall data were collected and compared against similar results for a plain airfoil (without Gurney flap) and against an airfoil with a variable-droop leading-edge shape [1]. Very-high-lift values may be achieved at relatively low angles of attack for an airfoil equipped with a Gurney flap. This increase in lift forces may be used to improve the autorotative performance of the rotor and may be exploited for individual blade control or onboard control of the rotor.

The present authors have recently studied the steady and unsteady load characteristics of a VR-12 airfoil with and without the Gurney flap [2]. It was found that the use of a Gurney flap could improve the static lift characteristics giving rise to a higher $C_{l,\max}$ (close to 1.8) compared to the conventional airfoil (close to 1.4). The dynamic stall characteristics of the Gurney-flap-equipped sections were not sufficiently different from that of a VR-12 airfoil, however.

In a follow-up study, the present researchers and their coworkers examined the beneficial effects of Gurney flaps on helicopter rotors in descent [3]. It was found that an existing rotor (similar to that used in BO-105), when retrofitted with a Gurney flap, could dramatically improve the thrust characteristics. It was found that the autorotative characteristics of the rotor (where a portion of the lift is tilted forward, causing an induced thrust rather than induced drag) could be improved with a Gurney-flap-equipped rotor.

The present work builds on the preliminary work reported in [3] for rotors in autorotative descent at fixed control setting. One of the objectives of the present work is to determine how the autorotative performance is affected if the Gurney-flap-equipped rotor is trimmed to the same hub forces and moments as the baseline rotor. A second objective of this work is to study the effects of Gurney flaps on blade loads and performance in steady level flight. Specifically, the effects of the Gurney flap on the blade root loads and hub vibratory loads are examined.

II. Computational Method and Validation Studies

A hybrid three-dimensional Navier–Stokes/free-wake method is used in this study. Modeling Gurney flaps required extensive modifications to the Navier–Stokes portion and, in particular, the single-block structure of the flow solver. Toward this end, the Navier–Stokes portion of this method has been replaced with a general-purpose multiblock solver called GENCAS (Generic Numerical Compressible Airflow Solver), developed by the first author [3,4]. This is a generic Reynolds-averaged Navier–Stokes solver that may be used to model a broad class of internal and external flows. This analysis solves the 3-D compressible viscous flow equations on a curvilinear body-fitted coordinate system. The baseline third-order upwind scheme was replaced with fifth- and seventh-order weighted essentially nonoscillatory (WENO5 and WENO7) flux reconstruction schemes. The baseline Spalart–Allmaras (SA) turbulence model was replaced with the SA-DES (detached eddy simulation) κ-ω model, a κ-ω/κ-ϵ blended model, and Menter's κ-ω shear stress transport model. Finally, the overall computational time

Presented as Paper 6726 at the 26th AIAA Applied Aerodynamics Conference, Honolulu, HI, 18–21 August 2008; received 30 October 2008; revision received 29 August 2009; accepted for publication 6 September 2009.

*Graduate Research Assistant, School of Aerospace Engineering. Student Member AIAA.
†Regents Professor and Associate Chair, School of Aerospace Engineering. Associate Fellow AIAA.
‡Professor, School of Aerospace Engineering. Associate Fellow AIAA.

required to perform the simulations was reduced by implementing a distributed computing approach based on a message-passing interface. The GENCAS solver, as a standalone solver, was validated for several 2-D AGARD standard test cases (e.g., RAE 2822 airfoil) and 3-D internal flow configurations (e.g., turbine guide vanes). In all of the calculations to be presented here, a third-order upwind scheme with a one-equation transport model for eddy viscosity, called the SA-DES model, was used.

In this hybrid approach, the time-consuming Navier–Stokes simulations are carried out only for a single blade, in a small region surrounding this reference blade (Fig. 1). The wake structure behind this reference blade and those of the other blades are modeled using a free-wake vortex model. Only the trailing vortices from the blade tips are modeled. The vortex strength of the most recently generated tip vortex segment was assumed to be peak bound circulation at the instance the vortex segment was generated. The tip vortices were propagated in time at a local velocity, calculated as the induced velocity due to all vortex filaments plus the freestream velocity. The induced velocities due to wake structure are also calculated at the Navier–Stokes (N-S) computational domain outer surface and applied as an inflow boundary condition. This allows the vortices to reenter the computational domain. If the rotor is in steady flight, only a single blade is modeled by the N-S solver, since the solution is periodic.

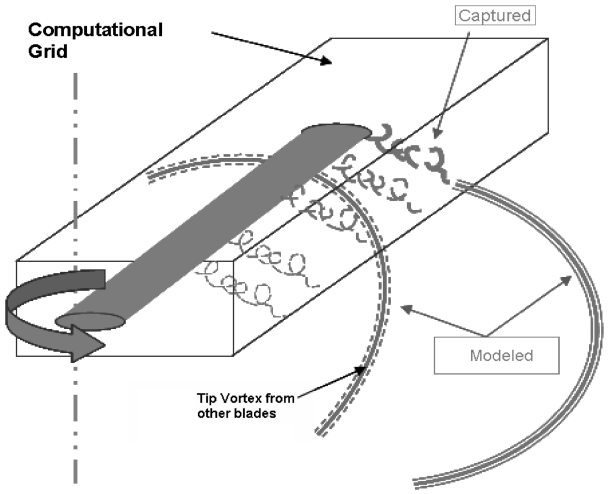

Fig. 1 A schematic view of the hybrid method [19].

At the start of the calculations, for the very first iteration, the wake is prescribed for five full revolutions. This initial guess reduces the N-S domain revolutions required to reach steady-state (periodic) solution. Subsequently, three–four additional revolutions were made to get the converged solution. The time step was chosen so that the blades rotated by 0.05 deg in the azimuthal direction. The wake structure was updated at every 5 deg.

A finite element solver called DYMORE is used in this study for modeling the aeroelastic response of the blades. DYMORE uses a multibody dynamics approach for the modeling of the rotor as a nonlinear elastic multibody system. This approach allows modeling of complex rotor configurations with emphasis on detail. The code incorporates robust and efficient time integration algorithms for integrating the resulting large-scale, nonlinear, differential, or algebraic equations. Figure 2 shows a multibody representation of a bearingless and articulated rotor system in DYMORE.

The calculations presented here exchange aerodynamic loads and deflections between the computational fluid dynamics (CFD) and computational structural dynamics (CSD) solvers at periodic intervals. The CFD/CSD coupling methodology framework is also shown in Fig. 2. The first step involves running the CSD code that computes airloads using its internal lifting-line-based aerodynamic model. These airloads are applied on the rotor structural model to compute the elastic deformations. The solver also trims the rotor to match the specified hub loads by adjusting the pitch controls. The periodic blade deformations obtained from this run are transferred to the CFD solver using a fluid–structure interface. The CFD solver deforms the blade mesh and computes the periodic airloads, which is subsequently transferred to the structural dynamics system using the delta airloads method, explained in detail in [5–8]. The delta airloads are first recast in a shaft-fixed frame as three components of forces and moments at each radial location before its use in the CSD analysis. The coupling iterations are executed until convergence is observed in hub loads obtained from the CFD solver and pitch controls obtained from the CSD solver. The coupling between DYMORE and the present CFD analysis uses the original fluid–structure interface (FSI) format to exchange data. Other comprehensive analyses (e.g., CAMRAD-II or RCAS) may also be used if desired.

The present coupled methodology has been validated with a companion hybrid CFD analysis called GT-Hybrid developed by the third author [9,10], before its use in the present study. Figure 3 shows the azimuthal variation of the airloads (lift and sectional pitching moment) at several radial locations for the UH-60A rotor in steady

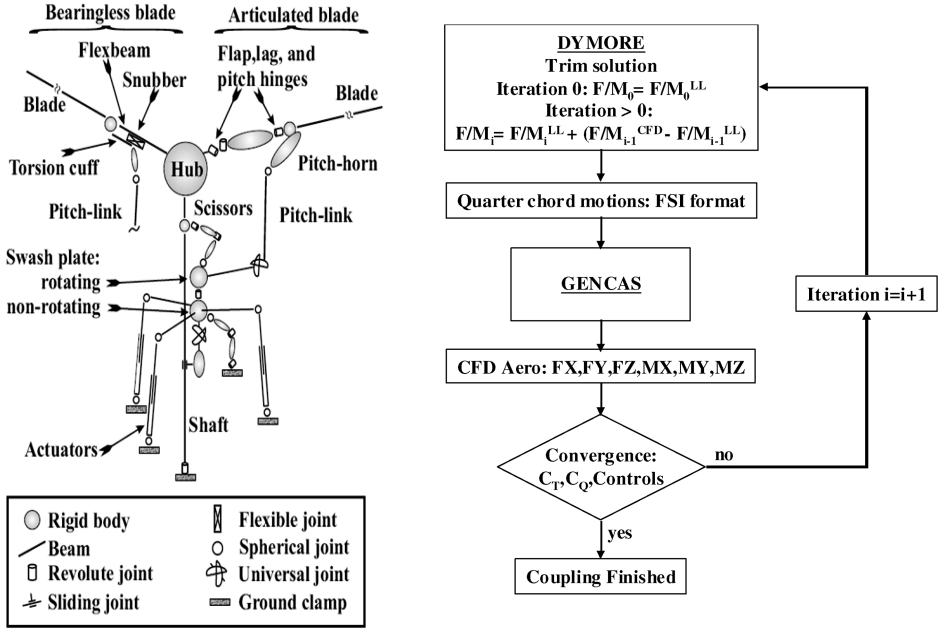

Fig. 2 Details of the multibody representation of a rotor system and the CFD/CSD coupling process.

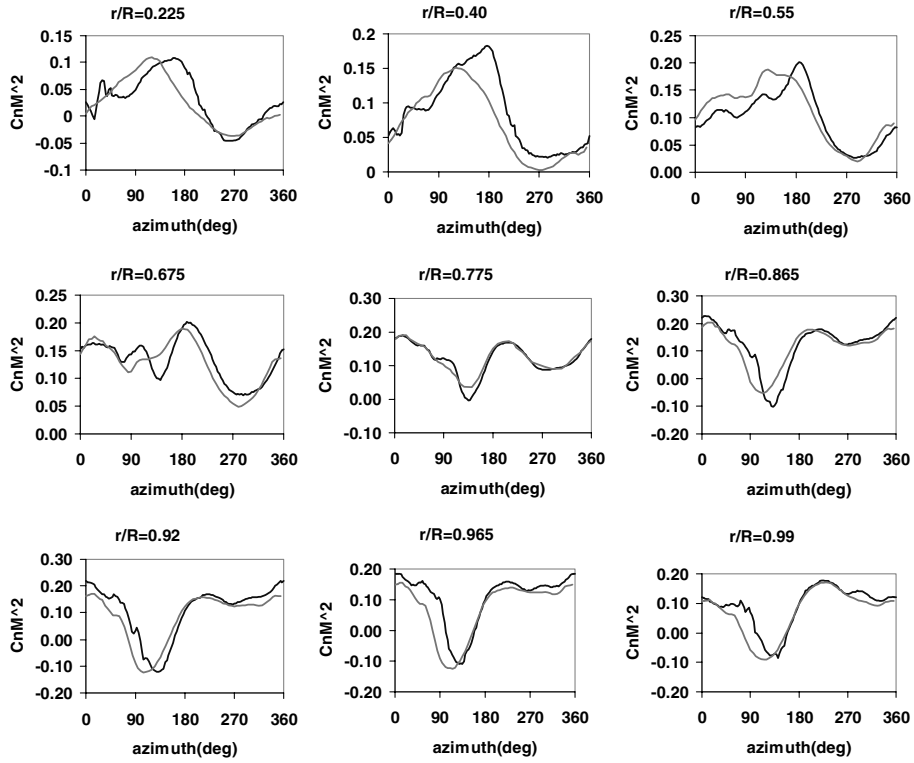

a) Normal forces

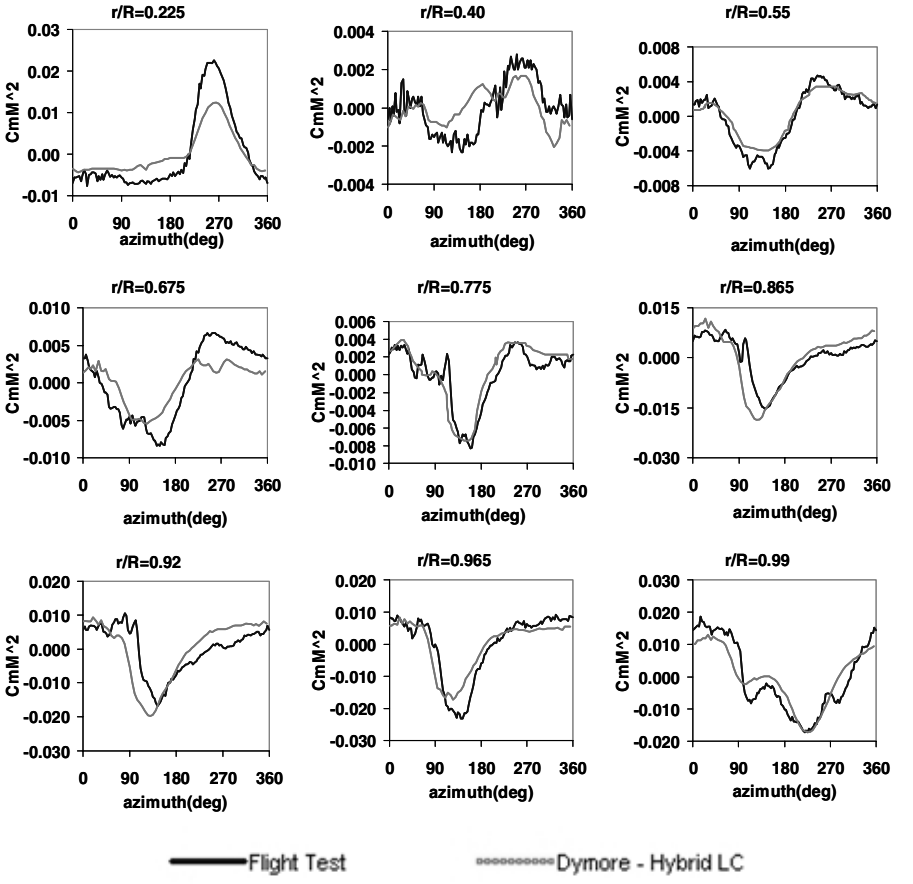

b) Pitching moments

Fig. 3 Sectional normal forces and pitching moments for a UH-60A rotor in steady level flight (counter C8534).

level flight. The flight condition is referred to as counter 8534 (advance ratio of 0.3675; C_T/σ of 0.084; tip speed of 725 ft/s, which corresponds to a tip Mach number of 0.642; and shaft angle of 7.3 deg relative to the direction of flight). It is shown that the simulations is in good agreement with measured loads.

For additional details on the coupling process and a detailed validation of the present hybrid methodology to rotors in forward flight, the reader is referred to [3,10]. This methodology has also been validated for horizontal-axis wind turbines for a range of wind speeds and yaw angles [11].

III. Results and Discussions

We now turn to the primary focus of the present study: the effects of Gurney flaps on the autorotative descent and forward-flight characteristics of a helicopter rotor. In this study, the BO-105 rotor was chosen because it is representative of rotors found on modern commercial rotorcraft. The blade elastic characteristics correspond to those of a model BO-105 rotor tested at the DNW tunnel [12].

A C-H type of grid system with $131 \times 65 \times 45$ (chordwise, spanwise, and surface normal direction) points (Fig. 4) is used, and 48 grid segments in the spanwise direction were placed on the blade surface. Boundary conditions applied are shown in Fig. 4. Flow properties were extrapolated from computational domain at inboard. Induced velocity due to wakes was added to grid velocity at the far field and outboard surface and then a characteristic-based non-reflecting boundary condition was applied.

Dynamic deployment of the Gurney flap was simulated via a dynamic wall boundary condition using the grid system shown in Fig. 4. If the Gurney flap is not deployed, the vertical 1.5%-chord-length portion behind the trailing edge becomes an extension of the wake cut, and a fluid interface boundary condition enforcing continuity of the flow properties is applied. When the reference blade

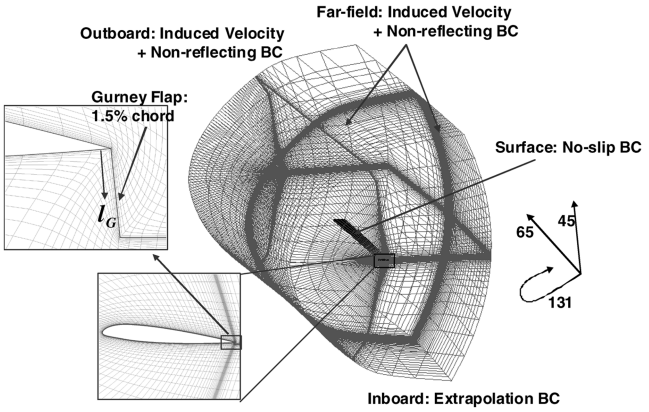

Fig. 4 Grid system for Gurney flap simulation (BC denotes boundary condition).

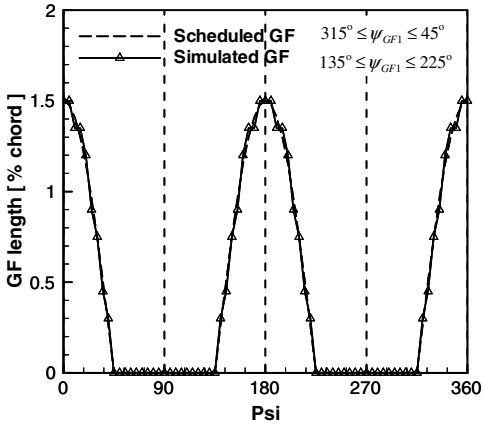

Fig. 5 Sample Gurney flap deployment schedule (2/rev).

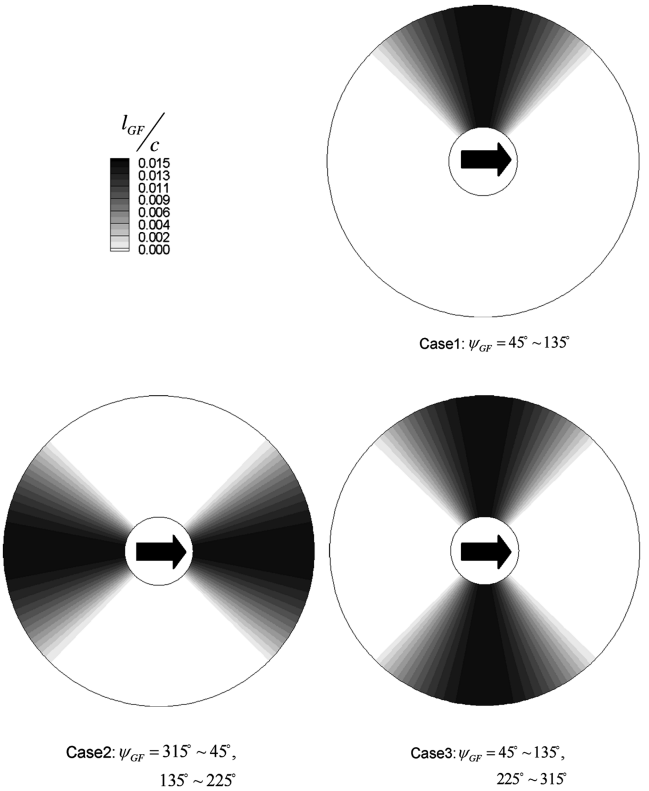

Fig. 6 Gurney flap schedule of each case.

reaches a prespecified azimuthal interval, the Gurney flap is deployed and no-slip boundary conditions are employed. The length of the deployed Gurney flap is assumed to follow a sinusoidal variation over the azimuthal interval where the flap is deployed. Figure 5 shows an example of simulated Gurney flap schedule, deployed twice per revolution (2/rev). Figure 6 shows three different Gurney flap schedules investigated in this study. In the present study, the Gurney flap is deployed over the entire span of the rotor. It is relatively straightforward to restrict its deployment to a portion of the rotor blade.

A. Effects of Gurney Flaps on Rotors in Steady Level Flight

In the first sequence of calculations, the BO-105 rotor equipped with a Gurney flap was studied in steady level flight. Three different Gurney flap schedules were explored and compared with the baseline case, giving rise to a total of four simulations. The four cases are summarized in Table 1.

In each of these cases, the CFD/CSD coupling was carried out using the methodology shown in Fig. 2, until the baseline rotor and the Gurney-flap-equipped rotor reached the same trim state, same user-specified thrust coefficient of 0.0069, and zero hub moments. Figure 7 shows the azimuthal variation of the blade pitch (including the collective) at the 75% radius, at the end of the coupled CFD/CSD

Table 1 Trimmed results

Case	$C_T \times 10^3$	$C_P \times 10^4$	PL	$L/D_e = L/[D + \frac{M_t \Omega}{V_\infty}]$
Baseline	6.91	3.56	19.4	2.93
Case 1: ψ_{GF} = 45–135 deg	6.93	3.42	20.26	3.07
Case 2: ψ_{GF} = 315–45 deg, 135–225 deg	6.91	3.36	20.56	3.10
Case 3: ψ_{GF} = 45–135 deg, 225–315 deg	6.94	3.44	20.15	3.04

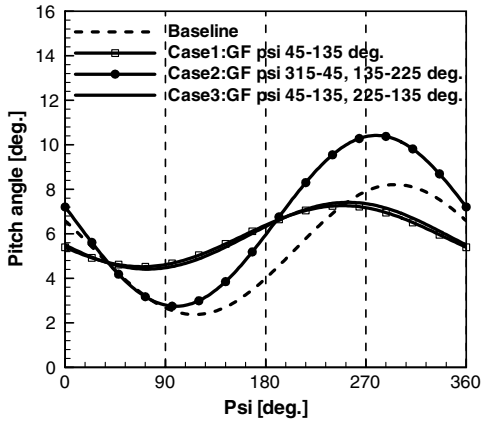

Fig. 7 Variation of blade pitch angle at 75% *R* at the end of CFD/CSD trim for the four cases.

trim process. As shown in Fig. 7, holding the flight conditions fixed and operating at the same thrust setting with deployment of Gurney flaps altered the trim state. The new trim states changed the distribution of induced velocity, sectional lift, and drag. As a result, the nondimensional power loading C_T/C_P and equivalent rotor L/D_e both show small differences compared to the baseline, as shown in Table 1. In this particular study under the given flight condition, dynamic deployment of a Gurney flap resulted in a slight decrease in rotor power. Similar power reductions were observed in other studies that used a Gurney flap [13], actively controlled flap [14,15], and higher harmonic control [16–18].

We next study the effects of the Gurney flap deployment on the hub loads. Recall that in the first case, the Gurney flaps are deployed only over the advancing side (between 45 and 135 deg azimuth). In the second case, the Gurney flap is deployed when the blades are in the fore and aft portions of the rotor disk, increasing the lift over those portions. The third case studied is where the Gurney flaps are deployed on the right and left portions of the rotor disk.

To maintain the rotor at the same trim state, the control system and the blade itself respond aeroelastically to counteract the effects of the Gurney flaps, at least in the time-averaged sense. In Fig. 8, it is observed that the thrust force averages out to the same azimuthally averaged target value of 5000 N, with zero hub pitching and rolling moment. The 4/rev and higher harmonics remain unaffected by the trimming process, however, leading to interesting variations in the hub loads, as shown Fig. 8.

We first look at the vibratory loads in the vertical direction (normal to the flight direction). It is shown that all four cases trim to the same averaged mean lift force of ∼5000 N. A 4/rev variation in loads attributable to the four blades is also clearly shown. The baseline rotor had a variation between 4760 and 5200 N, giving rise to a peak-to-peak

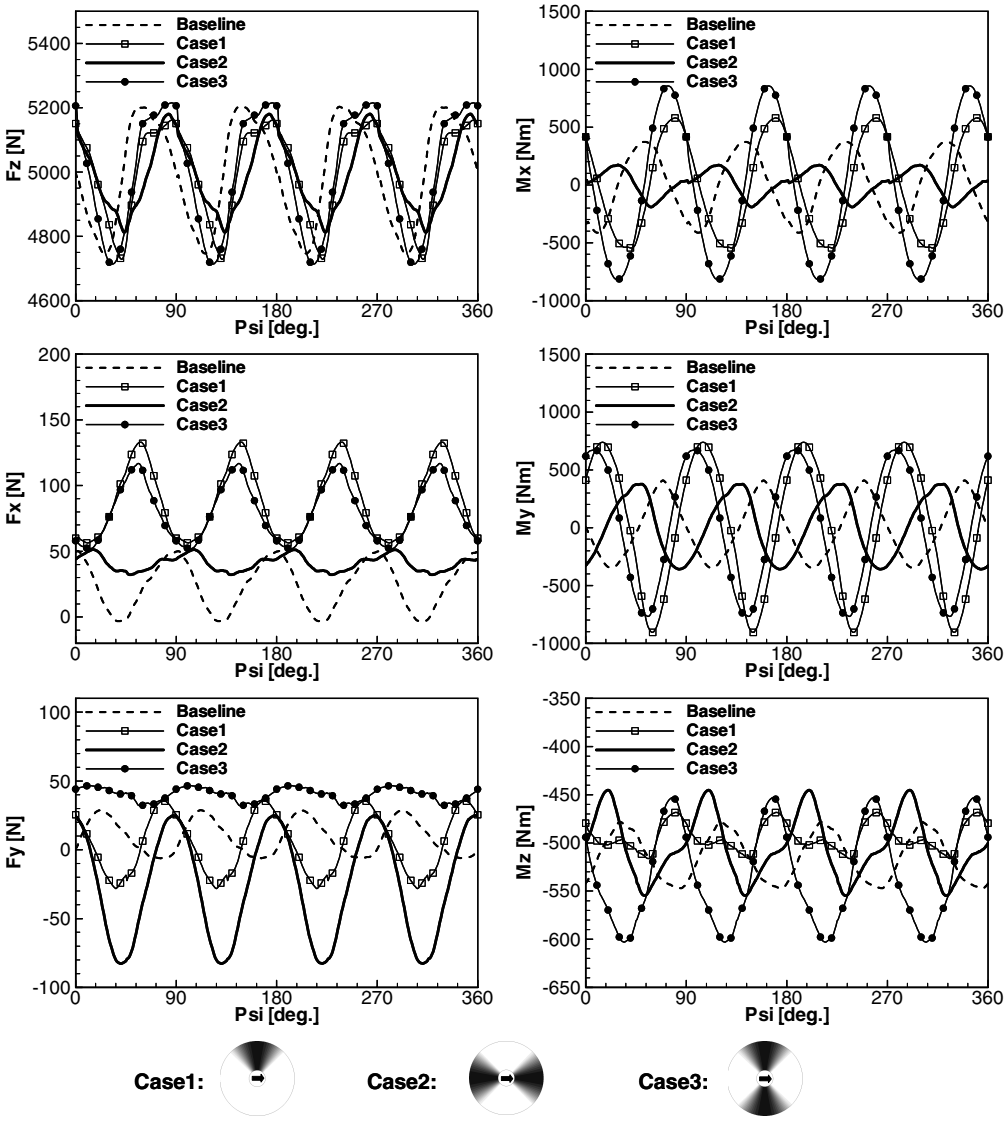

Fig. 8 Azimuthal variation of the hub loads in the inertial frame for the four cases.

variation of approximately 440 N. Case 1, in which the Gurney flap was deployed only between 45 and 135 deg on the advancing side, had a comparable peak-to-peak variation (between 4730 and 5170 N). In case 3, in which the Gurney flap is deployed on both the advancing side (between 45 and 135 deg azimuth) and retreating side (225 and 315 deg), the loads varied between 4720 and 5210 N. Case 2, in which the Gurney flap is deployed over the front (135 to 225 deg azimuth) and aft portion (315 to 45 deg azimuth), gave the lowest peak-to-peak loads (4820 to 5170 N).

We next look at the variation of the H force of the entire rotor. The baseline rotor had the lowest azimuthally averaged value of 26 N and a peak-to-peak +49 to −3 N. When the Gurney flap was deployed on the advancing side (case 1), or on both the advancing and retreating sides (case 3), the H force increased both in magnitude and peak-to-peak variations. In case 2, the time-averaged H force was higher at 42 N, but the peak-to-peak values were smaller (varying between 50 and 34 N).

We next look at the Y-force variations. The baseline Y force varied between +28 and −6 N, with a mean side force of 17 N. Case 3, in which the flap is deployed on the advancing and retreating sides, had a higher mean value, but the peak-to-peak variations were small. Case 2, in which the Gurney flaps are deployed on the front and aft portions of the rotor disk, gave significant variation in local sectional drag forces. Since a significant portion of this drag force is pointed along the Y axis, the net effect is to produce a large peak-to-peak variation of the Y force.

The effects of the Gurney flap deployment on the hub rolling and pitching moments as well as the shaft torque can similarly be examined. As shown in Fig. 8, case 1 and case 3 tend to give higher peak-to-peak rolling moments compared to the baseline case, although the mean values trim out to zero. Case 3 has hub rolling and pitching moment variations that are comparable to, if not smaller than, those for the baseline rotor.

In some applications, especially for hingeless rotors, it is highly desirable that the flexbeam loads and moments be reduced, both in mean values and the peak-to-peak variations. The present methodology allows the aerodynamic loads, structural loads, and blade deformations to be monitored virtually anywhere on the rotor system for these purposes. Figure 9 shows the variation in the aerodynamic loads at an arbitrarily selected sensor location on the flexbeam. It should be possible to monitor the loads and optimize the Gurney flap deflections to reduce the loads, deformations, and stress levels. Among the four cases studied, case 3 tended to have the largest peak-to-peak variations in the loads.

B. Effects of Gurney Flaps on the Autorotative Descent of Rotors

We next look at the effects of Gurney flaps on autorotative descent. The BO-105 rotor was considered again. In this study, the Gurney flaps were permanently deployed. In autorotative descent without power, there will not be enough control power available for periodic deployment of these devices. To simplify the analysis, all the calculations were done for a rigid rotor with a rigid Gurney flap. Several different flap settings were examined.

When the Gurney flaps are deployed, the blade sections generate higher lift force than would the baseline section. If the descent rate is high enough so that a portion of this lift force is pointing forward, as

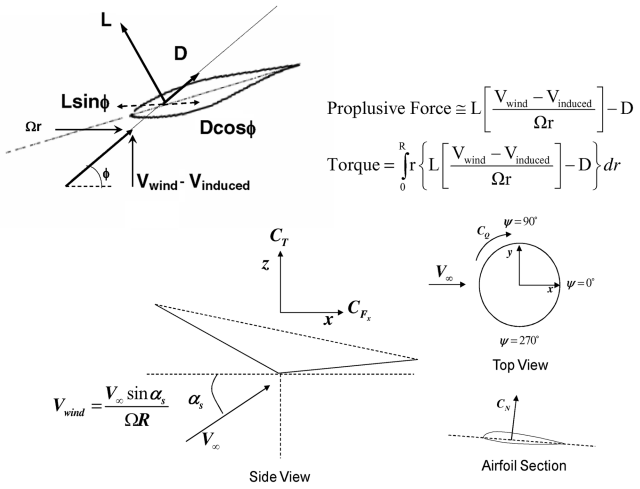

Fig. 10 Autorotation of a rotor in descent.

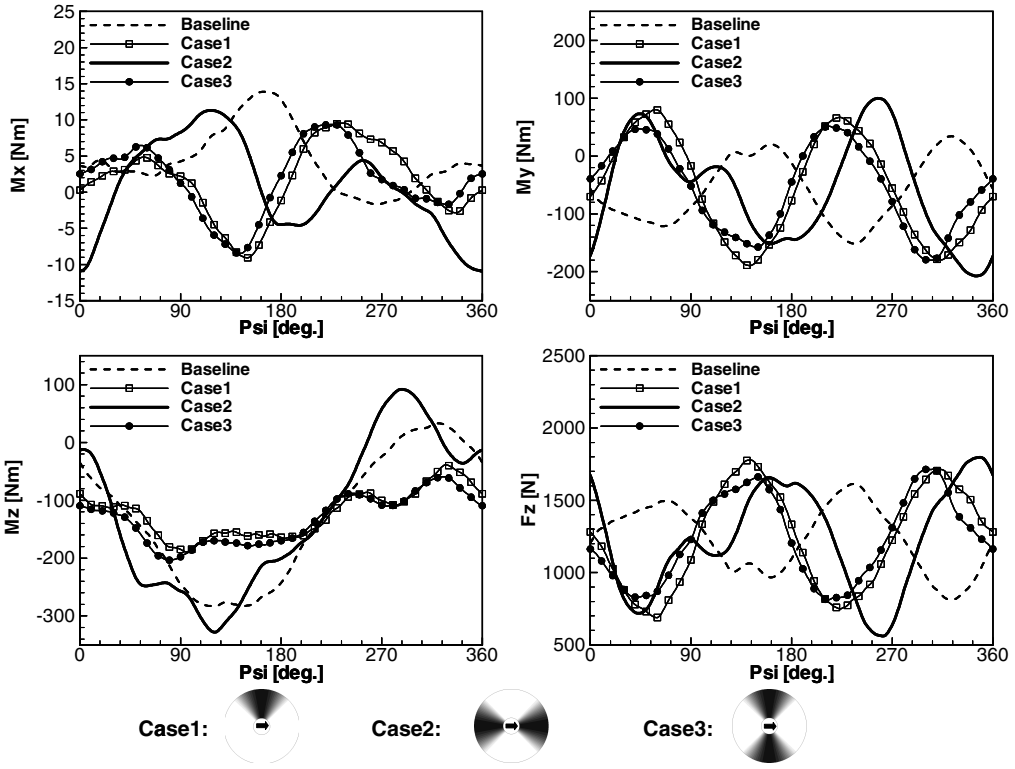

Fig. 9 Azimuthal variation of the flexbeam loads in the rotating frame for the four cases.

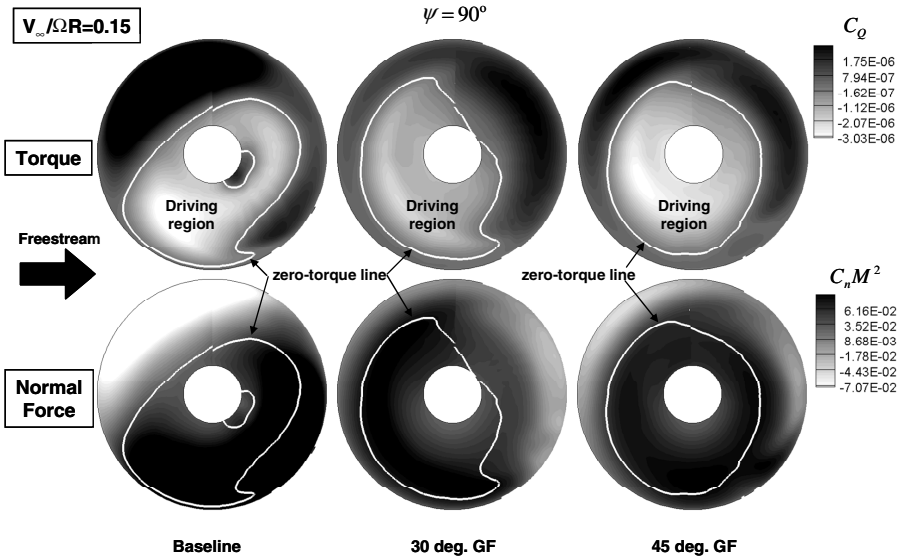

Fig. 11 Effects of Gurney flap on azimuthal distribution of normal forces and torque consumed for three different Gurney flap angles.

shown in Fig. 10, the blade will enter the windmill state and autorotate.

The analyses were done as follows. The rotor rpm (and hence the tip Mach number of the rotor) was held fixed. The advance ratio was parametrically varied between 0.1 and 0.2 in 0.05 increments. Only the 0.15 advance ratio case is discussed here, for brevity. The target C_T/σ of the baseline rotor (i.e., without a Gurney flap) was nominally set at 0.047, representative of the typical operating condition of a helicopter. In all three cases reported here (baseline rotor and rotors with Gurney flaps set at 30 and 45 deg angles relative to the chord line), the collective pitch and the cyclic pitch were iteratively adjusted until C_T/σ reached the target value and the azimuthally averaged rotor rolling and pitching moments at the hub were driven to zero. Although the freestream velocity was held constant, the shaft angle of attack was iteratively adjusted along with control inputs until the autorotative state was established where the torque converges to zero. The elastic deformations were ignored for this preliminary study, and the calculations were carried out in the rigid rotor mode.

Figure 11 shows the azimuthal and radial variation of the normal forces and torque consumption/production distributions for the 0.15 advance ratio case. All of the cases trim to the same C_T/σ, zero hub moments and zero total torque. This information may be fed into a CSD analysis to extract structural responses and to monitor blade and root stresses, if desired. It is interesting to examine which parts of the rotor disk are responsible for torque production and which parts of the rotor disk consume torque. It is shown in Fig. 11 that much of the aft side of the rotor disk is driven (i.e., consume torque), whereas much of the front half of the rotor disk is driving (produces torque), with the exception of the tip regions.

Of more interest is the vertical descent rate needed to maintain autorotative state at a given thrust setting and forward speed. Table 2 shows these results. It is shown that the vertical descent rate may be reduced with a modest 30 deg Gurney flap by approximately 40%. Increasing the flap angle to 45 deg causes local separation on the leeward side of the Gurney flap (see Fig. 12) and increases the section drag somewhat, leading to a higher descent rate than the 30 deg flap case.

Table 2 Effect of Gurney flap on the vertical descent rate needed to sustain autorotation (zero torque)

Thrust and descent rate	Baseline	30 deg GF	45 deg GF
C_T	3.6×10^{-03}	3.6×10^{-03}	3.8×10^{-03}
α_s, deg	28.9	17.5	25.0
$V_\infty \sin(\alpha_s)/(\Omega R)$	0.0735	0.0457	0.0642

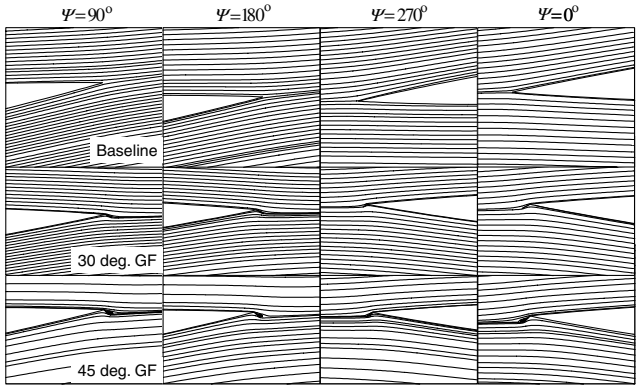

Fig. 12 Streamlines in the vicinity of the Gurney flap for the BO-105 rotor in autorotative descent.

IV. Conclusions

Navier–Stokes simulations have been carried out for an existing rotor retrofitted with a Gurney flap. The steady level flight loads and autorotative characteristics have been examined. In forward flight, for identical thrust and hub moment settings, it was found that the deployment of the flap significantly alters the vibratory load characteristics of the rotor. Deploying the Gurney flaps in the fore and aft portions of the rotor disk had the largest reduction in peak-to-peak vertical load fluctuations compared to the baseline case. Other deployment schedules were modestly beneficial in reducing the H force, Y force, and peak-to-peak variations in hub rolling and pitching moments. By judiciously combining the flap schedules, and possibly through the use of individual onboard control of the flaps, it should be possible to reduce the vibratory loads of the rotor. The Gurney flap was deployed over the entire blade span in this study. Placing the Gurney flaps only over the outboard radial locations should retain the benefits of this concept while improving the efficiency. The deployment of the Gurney flaps showed a slight decrease in power consumption.

In autorotative flight, deployment of Gurney flaps can increase the thrust coefficient during the flare maneuver decelerating the vehicle before touchdown. For a fixed thrust setting, use of Gurney flaps decreased the descent rate needed to maintain autorotation. Gurney flaps with moderate angles relative to the chord line were more effective in improving the autorotative performance than flaps that are placed at higher angles relative to the chord line, due to the presence of separated flow aft of the Gurney Flap and the attendant drag rise.

Acknowledgment

This work was funded by NASA Cooperative Agreement NNX07AP33A entitled "Flight Mechanics and Control Oriented Modeling for Next Generation On-Blade Control Concepts" with Wayne Johnson as Technical Monitor.

References

[1] Chandrasekhara, M. S., Martin, P. B., and Tung, C., "Compressible Dynamic Stall Performance of a Variable Droop Leading Edge Airfoil with a Gurney Flap," AIAA Paper 2004-0041, Jan. 2004.

[2] Guzel, G., Sankar, L. N., and Rhee, M., "Computational Investigation of the Effects of Gurney Flap on the Aerodynamic Performance of VR-12 Airfoil," AIAA Paper 2005-4960, June 2005.

[3] Min, B. Y., Sankar, L. N., and Yu, Y. H., "Computational Studies of the Effects of Gurney Flaps on the Autorotative Performance of Rotors in Descent Flight," *AHS Aeromechanics Specialists Meeting* [CD-ROM], AHS International, Alexandria, VA, Jan. 2008.

[4] Min, B. Y., Lee, W., Englar, R., and Sankar, L. N., "Numerical Investigation of Circulation Control Airfoils," *Journal of Aircraft*, Vol. 46, No. 4, July–August 2009, pp. 1403–1410. doi:10.2514/1.41638

[5] Sitaraman, J., "CFD Based Unsteady Aerodynamic Modeling for Rotor Aeroelastic Analysis," Ph.D. Dissertation, Department of Aerospace Engineering, Univ. of Maryland, College Park, MD, 2003.

[6] Datta, A., Sitaraman, J., Chopra, I., and Baeder, J. D., "CFD/CSD Prediction of Rotor Vibratory Loads in High-Speed Flight," *Journal of Aircraft*, Vol. 43, No. 6, Nov.–Dec. 2006, pp. 1698–1709. doi:10.2514/1.18915

[7] Datta, A., and Chopra, I., "Prediction of UH-60A Dynamic Stall Loads in High Altitude Level Flight using CFD/CSD Coupling," *AHS Aeromechanics Specialists Meeting* [CD-ROM], AHS International, Alexandria, VA, June 2005.

[8] Potsdam, M., Yeo, H., and Johnson, W., "Rotor Aerodynamic Prediction Using Loose Aerodynamic/Structural Coupling," *AHS Aeromechanics Specialists Meeting* [CD-ROM], AHS International, Alexandria, VA, June 2004.

[9] Rajmohan, N., "Application of Hybrid Methodology to Rotors in Steady and Maneuvering Flight," Ph.D. Dissertation, School of Aerospace Engineering, Georgia Inst. of Technology, Atlanta (to be published).

[10] Rajmohan, N., Sankar, L. N., Bauchau, O., Makinen, S. M., Egolf, T. A., and Charles, B. D., "Application of Hybrid Methodology to Rotors in Steady and Maneuvering Flight," *AHS Aeromechanics Specialists Meeting* [CD-ROM], AHS International, Alexandria, VA, 2008.

[11] Tongchitpakdee, C., Benjanirat, S., and Sankar, L. N., "Numerical Studies of the Effects of Active and Passive Circulation Enhancement Concepts on Wind Turbine Performance," AIAA Paper 2006-0198, Jan. 2006.

[12] Yu, Y. H., Tung, C., van der Wall, B. G., Pausder, H., Burley, C., Brooks, T., Beaumier, P., Delrieux, Y., Mercker, E., and Pengel, K., "The HART-II Test: Rotor Wakes and Aeroacoustics with Higher-Harmonic Pitch Control (HHC) Inputs—The Joint German/French/Dutch/US Project," *AHS Aeromechanics Specialists Meeting* [CD-ROM], AHS International, Alexandria, VA, June 2002.

[13] Yeo, H., "Assessment of Active Controls for Rotor Performance Enhancement," *Journal of the American Helicopter Society*, Vol. 53, No. 2, April 2008, pp. 152–163. doi:10.4050/JAHS.53.152

[14] Glaz, B., Friedmann, P. P., and Liu, L., "Vibration Reduction and Performance Enhancement of Helicopter Rotors Using an Active/Passive Approach," AIAA Paper 2008-2178, April 2008.

[15] Liu, L., Friedmann, P. P., Kim, I., and Bernstein, D. S., "Rotor Performance Enhancement and Vibration Reduction in Presence of Dynamic Stall Using Actively Controlled Flaps," *Journal of the American Helicopter Society*, Vol. 53, No. 4, Oct. 2008, pp. 338–350. doi:10.4050/JAHS.53.338

[16] Shaw, J., Albion, N., Hanker, E. J., Jr., and Teal, R. S., "Higher Harmonic Control: Wind Tunnel Demonstration of Fully Effective Vibratory Hub Force Suppression," *Journal of the American Helicopter Society*, Vol. 34, No. 1, Jan. 1989, pp. 14–25. doi:10.4050/JAHS.34.14

[17] Nguyen, K., and Chopra, I., "Effects of Higher Harmonic Control on Rotor Performance and Control Loads," *Journal of Aircraft*, Vol. 29, No. 3, May–June 1992, pp. 336–342. doi:10.2514/3.46166

[18] Cheng, R. P., and Celi, R., "Optimum Two-Per-Revolution Inputs for Improved Rotor Performance," *Journal of Aircraft*, Vol. 42, No. 6, Nov.–Dec. 2005, pp. 1409–1417. doi:10.2514/1.20884

[19] Tongchitpakdee, C., "Computational Studies of the Effects of Active and Passive Circulation Enhancement Concepts on Wind Turbine Performance," Ph.D. Dissertation, School of Aerospace Engineering, Georgia Inst. of Technology, Atlanta, 2007.